The effect of lithium surface coatings on plasma performance in the National Spherical Torus Experiment[a)]

H. W. Kugel,[1,b)] M. G. Bell,[1] J.-W. Ahn,[2] J. P. Allain,[3] R. Bell,[1] J. Boedo,[2] C. Bush,[4] D. Gates,[1] T. Gray,[1] S. Kaye,[1] R. Kaita,[1] B. LeBlanc,[1] R. Maingi,[4] R. Majeski,[1] D. Mansfield,[1] J. Menard,[1] D. Mueller,[1] M. Ono,[1] S. Paul,[1] R. Raman,[5] A. L. Roquemore,[1] P. W. Ross,[1] S. Sabbagh,[6] H. Schneider,[1] C. H. Skinner,[1] V. Soukhanovskii,[7] T. Stevenson,[1] J. Timberlake,[1] W. R. Wampler,[8] and L. Zakharov[1]
[1]*Princeton Plasma Physics Laboratory, Princeton, New Jersey 08543, USA*
[2]*University of California at San Diego, La Jolla, California 92093, USA*
[3]*Purdue University, School of Nuclear Engineering, West Lafayette, Indiana 47907, USA*
[4]*Oak Ridge National Laboratory, Oak Ridge, Tennessee 37831, USA*
[5]*University of Washington, Seattle, Washington 98195, USA*
[6]*Columbia University, New York, New York 10027, USA*
[7]*Lawrence Livermore National Laboratory, Livermore, California 94551, USA*
[8]*Sandia National Laboratories, Albuquerque, New Mexico 87185, USA*

(Received 18 November 2007; accepted 17 March 2008; published online 2 May 2008)

National Spherical Torus Experiment [which M. Ono *et al.*, Nucl. Fusion **40**, 557 (2000)] high-power divertor plasma experiments have shown, for the first time, that benefits from lithium coatings applied to plasma facing components found previously in limited plasmas can occur also in high-power diverted configurations. Lithium coatings were applied with pellets injected into helium discharges, and also with an oven that directed a collimated stream of lithium vapor toward the graphite tiles of the lower center stack and divertor. Lithium oven depositions from a few milligrams to 1 g have been applied between discharges. Benefits from the lithium coatings were sometimes, but not always, seen. These benefits sometimes included decreases in plasma density, inductive flux consumption, and edge-localized mode occurrence, and increases in electron temperature, ion temperature, energy confinement, and periods of edge and magnetohydrodynamic quiescence. In addition, reductions in lower divertor D, C, and O luminosity were measured.
 [DOI: 10.1063/1.2906260]

I. INTRODUCTION

The National Spherical Torus Experiment (NSTX)[1,2] research on lithium-coated plasma facing components (PFCs) is the latest step in a research program to develop liquid lithium for providing a self-healing plasma facing surface in a deuterium-tritium reactor.[3] The initial NSTX lithium research is aimed towards sustaining the plasma current noninductively in high confinement mode (H-mode) plasmas, which requires control of both secular density rises and impurity influxes. Motivated by the long range potential of lithium PFCs, NSTX has been investigating lithium coatings for density control and impurity control as part of a phased, three-part approach to lithium PFCs: First with lithium pellet injection, then with lithium evaporators, and finally with a liquid lithium divertor. This phased approach is allowing NSTX control systems, diagnostics, and research to be adapted to lithium-coated wall conditions. Under these conditions, deuterium ions and neutrals incident on solid lithium PFCs can react to form lithium deuteride (LiD), and remain sequestered in the lithium unavailable for recycling. This is in contrast to molecular deuterium, which does not react, and can recycle. This behavior of ions and neutrals provides a pumping effect over the plasma wetted area for a wide range in plasma density, shape, and position, and this is the basis for the control of wall recycling and impurities being investigated in this work.

In NSTX, recycling of hydrogenic species from the plasma contact with graphite surfaces, contributes to a secular density rise observed in most H-mode, neutral beam injection (NBI) heated plasmas. Experiments on the Tokamak Fusion Test Reactor (TFTR) obtained reduced recycling and significantly enhanced performance using lithium pellet injection (LPI), evaporation, and laser techniques to apply lithium to its graphite inner toroidal limiter, but only after it had been thoroughly degassed by repeated helium discharges.[4] This wall degassing is believed to prevent thin coatings of the applied lithium from combining with the fuel gas and impurities embedded in the graphite PFCs. Lithium reactions with gas embedded in the graphite (e.g., resulting in LiD, LiOH, LiOD, Li_2CO_3) make it unavailable to combine with incident deuterium ions and neutrals to form LiD, and are thereby unable to provide density pumping. In this work, the initial experiments involved thin solid lithium coatings, and used thoroughly degassed ("conditioned") graphite surfaces. The more recent experiments with thicker solid lithium coatings have not used degassed graphite surfaces.

The NSTX 2005 LPI (2005-LPI) results described below for the limiter plasmas are similar to the experience with

[a)]Paper TI2 6, Bull. Am. Phys. Soc. **52**, 276 (2007).
[b)]Invited speaker.

lithium coatings in TFTR[4] and with a liquid-lithium limiter in the Current Drive Experiment—Upgrade (CDX-U).[5] The NSTX 2005-LPI experiments extended the potential benefits of lithium surface coating for plasma density control to divertor plasmas, and suggested that additional lithium deposition could increase plasma density pumping and prolong its duration. This hypothesis motivated the development of a lithium evaporator for performing routine lithium coating over a significant fraction of the plasma facing surfaces.

II. EXPERIMENT DESCRIPTION

NSTX capabilities include $R_0 \leq 0.85$ m, $a \leq 0.67$ m, $R/a \geq 1.26$, $\kappa \leq 2.7$, $\delta \leq 0.8$, $I_p \leq 1.5$ MA, $B_T \leq 0.55$ T, and 1.5 s maximum pulse length.[1,2] Copper passive stabilizer plates, graphite power handling surfaces, 7 MW of deuterium neutral beam injection (NBI) heating, 6 MW of 30 MHz high harmonic fast wave (HHFW) for radio frequency (rf) heating and current drive provide additional experimental versatility. The 0.2 m radius center stack (CS) is clad with alternating vertical columns of 1.3 cm thick graphite (Union Carbide, type ATJ) tiles between columns of two-dimensional carbon fiber composite (Allied Signal, type 865-19-4) tiles. The inner divertor tiles are 5.1 cm thick type ATJ graphite; the outer divertor and passive stabilizer plate tiles are 2.5 cm thick type ATJ graphite. The PFCs are conditioned as required using vacuum bakeout at 350° C, helium glow discharge cleaning between discharges and boronization.[6] A sabot-style lithium pellet injector (LPI) can inject lithium, other low-Z pellets, or powders into edge plasmas.[7] The NSTX configuration enables experiments with ohmic, NBI, and HHFW rf heated discharges on CS limiter start-up plasmas, lower single-null diverted (LSND) plasmas, and double null diverted plasmas, with and without coaxial helicity injection. Figure 1 shows a poloidal cross section of NSTX, the upper divertor location of the lithium evaporator (LITER) at toroidal angle 165°, and the LITER aiming angles for the 2006 and 2007 campaigns, respectively. The red line indicates the last closed flux surface (LCFS) of the LSND deuterium reference discharges used for the LITER campaigns. Shown also are the upper and lower divertor locations of the two in-vessel quartz deposition monitors (QDMs) each at toroidal angle 225°. These QDMs were used as independent monitors of the lithium deposition rate between discharges as determined from the LITER oven temperature (described below).

A. LPI

The experimental configuration described in this section was used in the 2005–2007 experimental campaigns to obtain the results described below. The 2005-LPI campaign characterized the behavior of CS limited and LSND deuterium discharges (I_p=0.8 MA, P_{NBI}=4 MW, B_T=0.45 T) following LPI to coat well-degassed graphite surfaces. First, the plasma facing surfaces were conditioned with a series of helium discharges. Immediately thereafter, low velocity (~100 m/s) lithium pellets with masses 2 to 5 mg were injected 1 each, or 2 each, into 10 to 20 repeated ohmic helium discharges, to introduce a total of 24 to 30 mg of lithium on either the graphite CS limiter or the lower divertor.

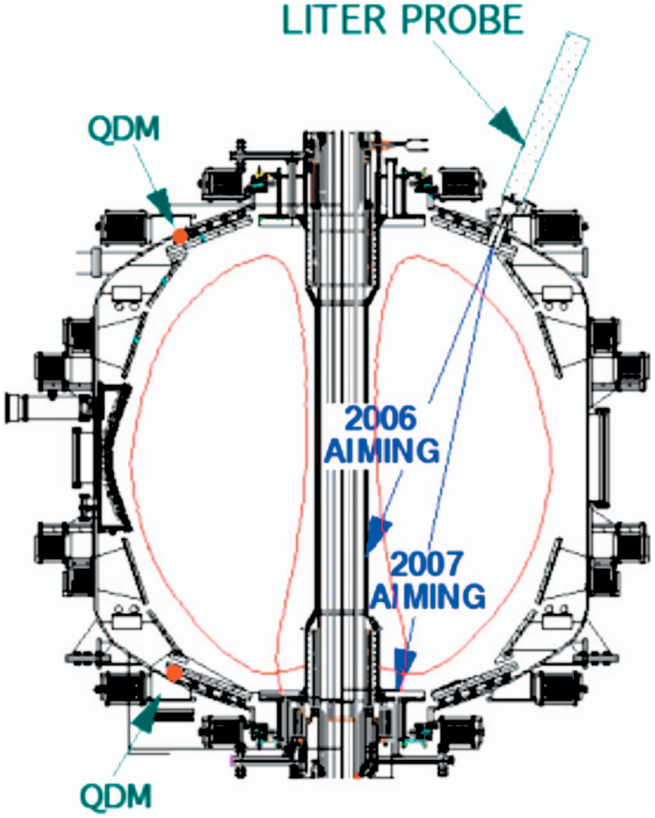

FIG. 1. (Color) Shown is a schematic diagram of the poloidal cross section of NSTX, the locations of the lithium evaporator (LITER) at toroidal angle 165°, and the aiming angles used for the 2006 and 2007 campaigns, respectively. Shown also are the two quartz deposition monitors, each at toroidal angle 225°, used as independent monitors of the lithium deposition rate as determined from the oven temperature. The red line indicates the LCFS of the LSND deuterium reference discharges used for the LITER campaigns.

B. LITER

Figure 2 shows a schematic diagram of the LITER evaporator. The unit has a 90 g lithium capacity. It consists of a main reservoir oven and an output duct to allow insertion in an available gap in the upper divertor region. The 2006 version was aimed 22° downward at the lower shoulder of the center stack; the 2007 version was aimed 12° downward toward the middle of the inner divertor as seen in Fig. 1. Two heaters were used: One heater on the output duct and one heater on the main reservoir. The heater on the main reservoir was typically operated to provide liquid lithium temperatures of 600–650 °C. The heater on the output duct was operated about 50–100 °C hotter than the heater on the main reservoir to reduce lithium condensation on the output duct aperture. The evaporation rate was computer controlled by varying the oven temperature. Typical evaporation rates have been in the range 1 to 40 mg/min. The evaporation rates were calibrated in NSTX laboratory measurements every 50 °C over the temperature range 550–650 °C. Figure 3 shows the results of a typical laboratory angular distribution

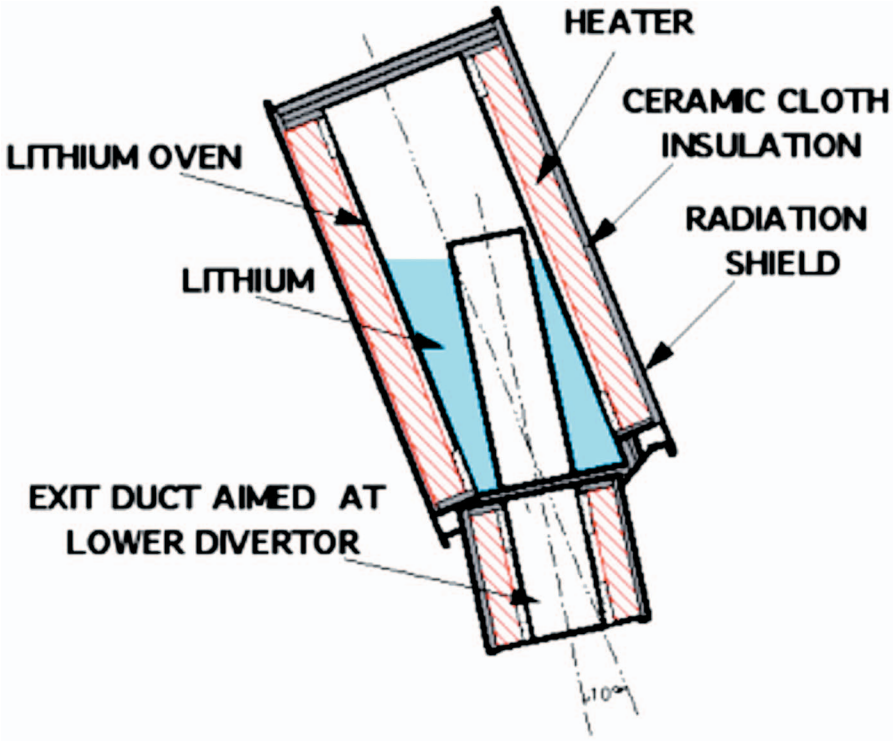

FIG. 2. (Color) Schematic diagram of the lithium evaporator (2007-LITER).

measurement using a scanning QDM that measured the output lithium beam to have a Gaussian half-width of approximately 5.9 cm at a distance of 30.2 cm. These angular distributions were integrated to obtain the total evaporation rate versus temperature. The results were in agreement with theoretical simulations.[8] A computer was used to control the oven temperature and to acquire the oven thermocouple temperature signals. The measured LITER oven temperatures were used together with the laboratory calibration measurements to determine the total evaporated lithium between discharges. Figure 4 shows a simulation of the lithium deposition in NSTX.

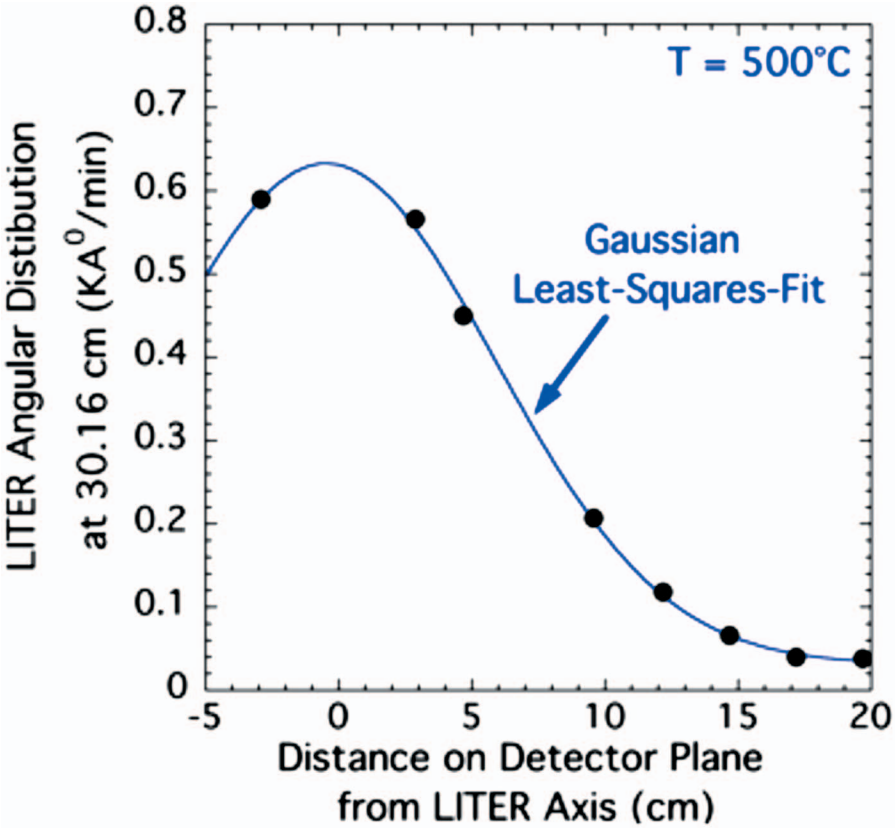

FIG. 3. (Color) The results of a typical laboratory angular distribution measurement of the output lithium beam at 500 °C using a scanning quartz deposition monitor. The measured angular distributions were found to be independent of temperature over the temperature range 450–650 °C.

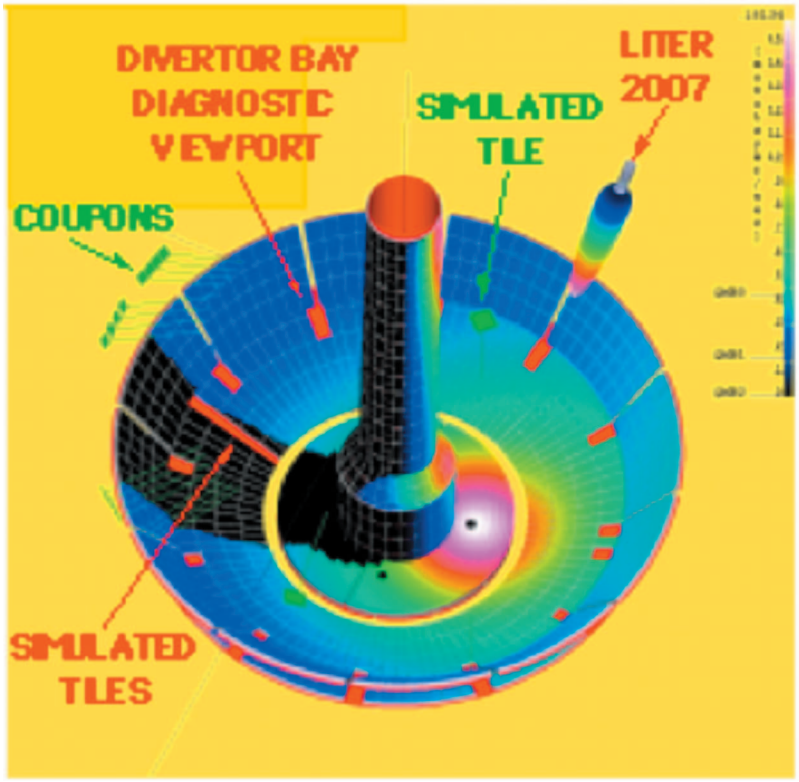

FIG. 4. (Color) Simulation of the evaporated lithium distribution over the NSTX lower divertor region showing the relative change in deposition thickness over the lower divertor region. Shown are the locations of the divertor viewports at each of the 12 bays, the locations of midplane coupons, and the divertor tiles used to compare the deposition simulation with results from nuclear reaction analysis.

1. 2006-LITER

The 2006-LITER campaign characterized initial low confinement mode (L-mode) and H-mode discharges on both conditioned and unconditioned graphite surfaces. As noted above, the 2006-LITER, lithium coatings were applied with LITER aimed to direct a collimated stream of lithium vapor toward the graphite tiles of the lower center stack and divertor (Fig. 1). Lithium depositions from a few milligrams to ~1 g were applied between discharges. The relatively low thermal inertia of 2006-LITER allowed cool-down in about 30–60 min, from temperatures (600–640 °C) yielding relatively high evaporation rates (10–20 mg/min) to below temperatures giving minimal evaporation (<375 °C). This cool-down allowed opening diagnostic window shutters without risk of lithium coating of windows, and in addition, allowed HeGDC to be performed separately from the lithium evaporation. About 12 separate depositions of lithium were performed onto the lower divertor prior to LSND NBI heated reference discharges (I_p=1 MA, P_{NBI}=4 MW, B_T=0.45 T). These individual depositions ranged from 1.6 mg to 4.8 g of lithium for a total of 9 g deposited by the end of the 2006 experimental campaign. This lithium amount would correspond to a thickness of 0.4 μm if averaged over the interior area of NSTX.

2. 2007-LITER

The 2006-LITER results suggested that higher evaporation rates could provide depositions well above any erosion-related threshold, and that evaporating up to, and during discharges would minimize effects related to possible lithium reactions with the graphite substrate and vacuum impurities. Hence, for the 2007-LITER campaign, LITER capacity was increased from 64 to 90 g, and was re-aimed toward the inner divertor for a threefold increase divertor target deposition. In addition, the LITER output aperture area was increased by a factor of 1.7, and heater improvements made to allow higher evaporation rates. These changes allowed an increased amount of lithium, and an increased rate of lithium deposited on the lower divertor target region between discharges. Typical evaporation rates of 10 to 40 mg/min were tested for a total lithium deposition of ~93 g by the end of the 2007-LITER campaign. This would correspond to a lithium thickness of 4.4 μm if averaged over the interior area of NSTX.

III. EXPERIMENTAL RESULTS

A. 2005-LPI L-mode results using degassed graphite

2005-LPI experiments[8] reproduced the low recycling reduction in L-mode plasmas first observed in TFTR.[4] Spectroscopic data indicated that the injected lithium was deposited primarily on the surfaces surrounding the plasma divertor contact area. In both the CS limited and lower divertor, LSND configurations, the first subsequent NBI heated L-mode deuterium reference plasma showed a reduction in the volume-averaged plasma density during the NBI heating by a factor of about 2 compared with the respective deuterium reference discharge before the lithium deposition. Figure 5 shows a comparison of the density profiles for the reference deuterium discharge before lithium and the first deuterium reference discharge immediately after LPI deposi-

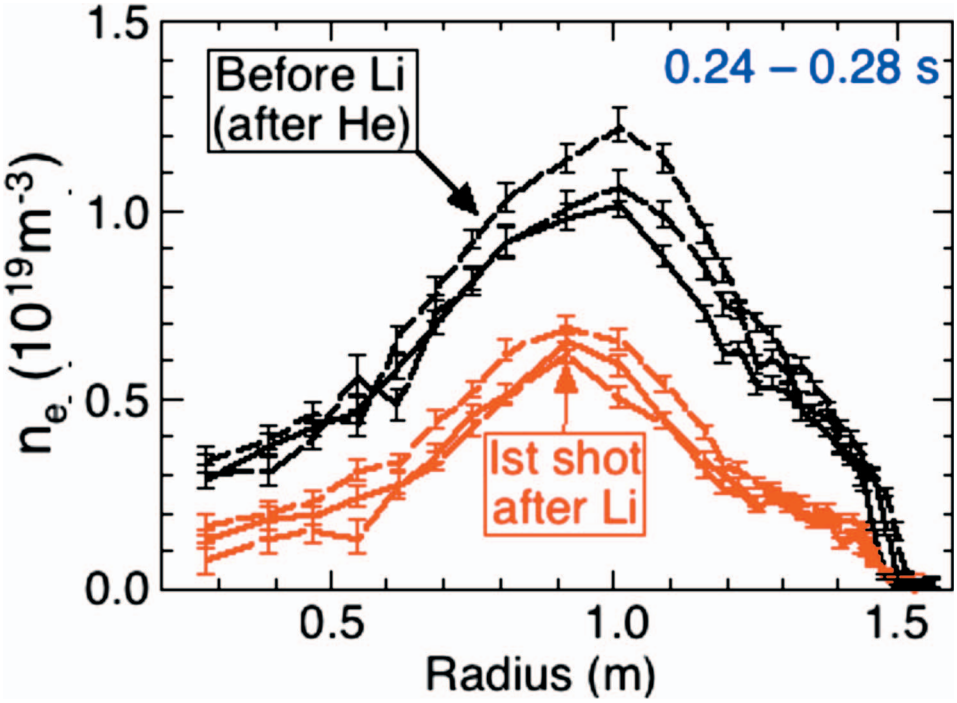

FIG. 5. (Color) A comparison of the density profiles for the reference deuterium discharge before lithium (black) and the first deuterium reference discharge immediately after LPI deposition of 25 mg (red). A reduction in the volume-averaged density by a factor of about 2 and profile shape changes occurred. The profile measurement times for both discharges are 0.243 s (solid), 0.260 s (longer dashes), 0.273 s (shorter dashes).

tion of 25 mg. A reduction in the volume-averaged density by a factor of about 2 and profile shape changes occurred. This density reduction was less on the next discharge and was not evident on the third discharge. The saturation of the apparent wall pumping can be understood if the effect occurs through the formation of LiD on the surface: The amount of lithium introduced could react with about 6–9 mg of deuterium, and about 3.5 mg of deuterium was injected on each discharge. The density in these discharges was chosen to be much less than typical L-mode discharges to provide a plasma particle content comparable to the available Li pumping capacity.

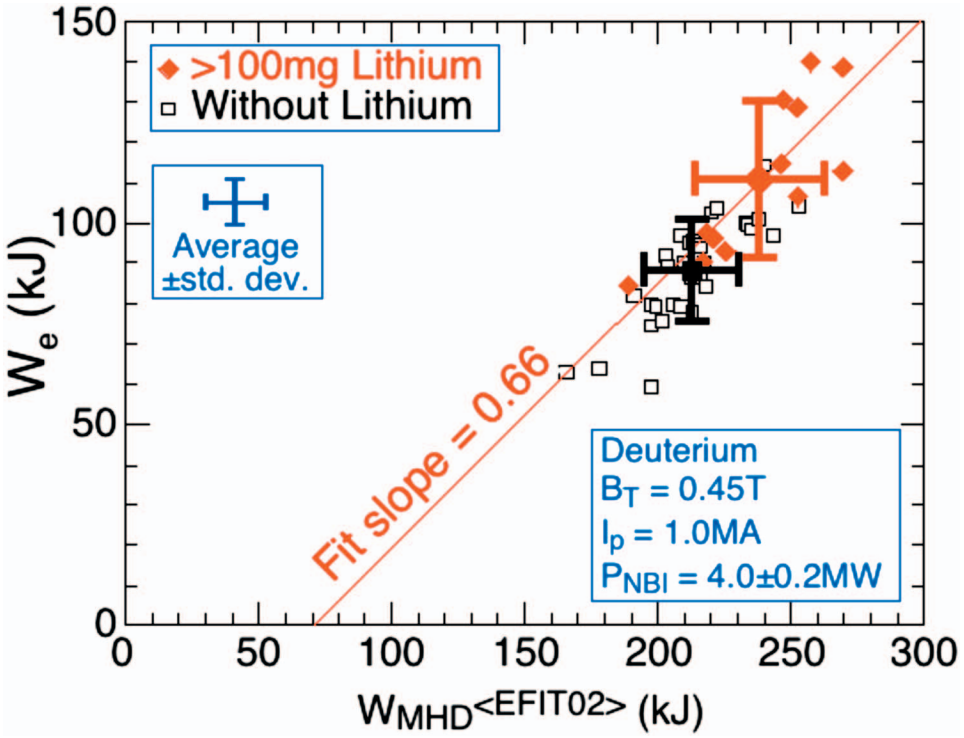

FIG. 6. (Color) The 2007 database of electron stored energy (W_e) vs total stored energy (W_{MHD}) for deuterium reference plasmas immediately following lithium deposition, and for deuterium reference plasmas prior to lithium deposition. EFIT02 is an equilibrium analysis constrained by external magnetics, electron profile shape, and diamagnetic flux.

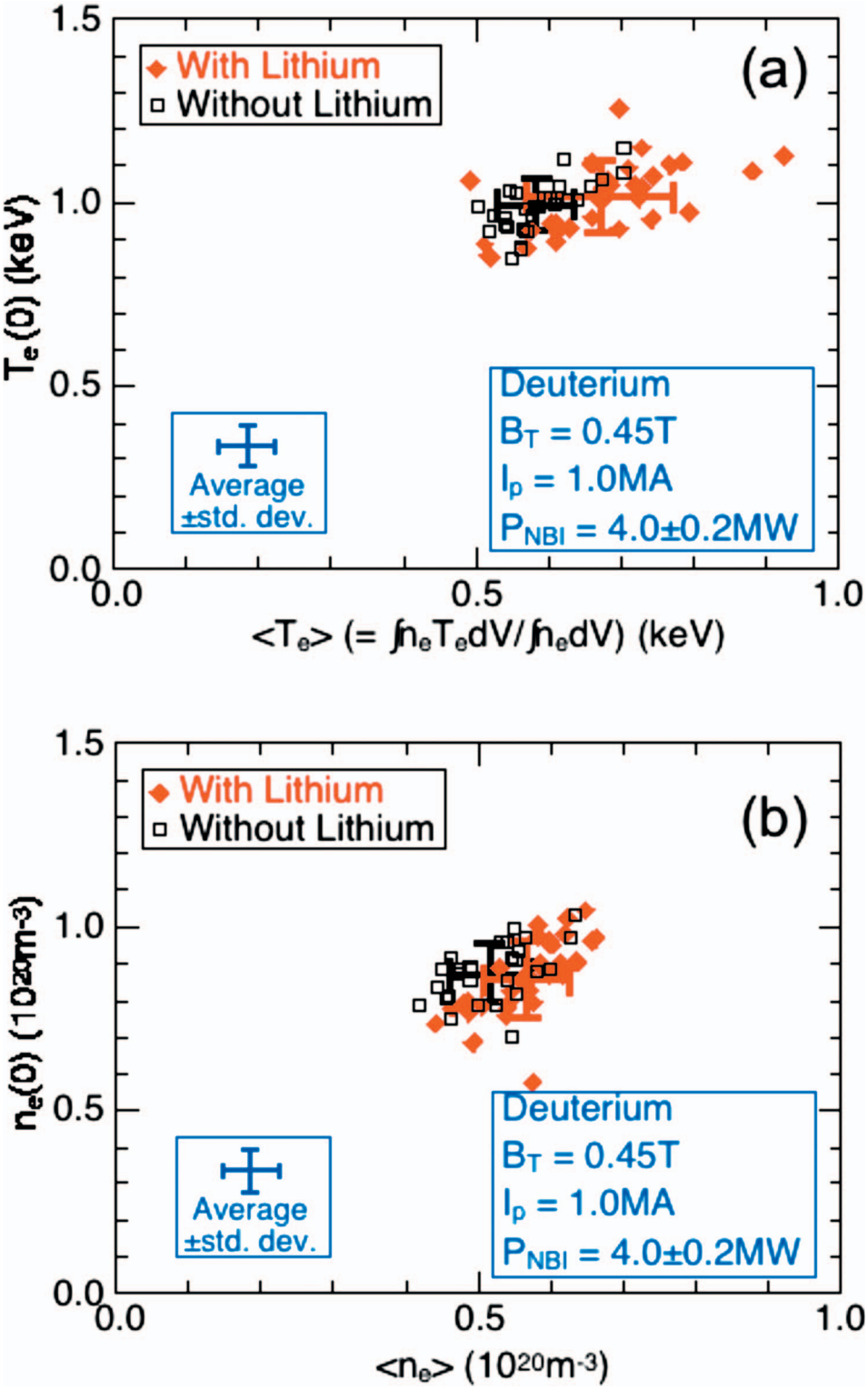

FIG. 7. (Color) Shown for the same discharges as in Fig. 6, are (a) the central electron temperature $[T_e(0)]$ vs the volume-averaged electron temperature $[\langle;T_e\rangle]$, and (b) the central density $[n_e(0)]$ vs the volume-averaged electron density $[\langle n_e\rangle]$.

B. Lithium evaporator results

1. 2006-LITER results for L-mode on unconditioned graphite

The 2005-LPI results implied that thicker lithium coatings would not be as susceptible to the condition of the graphite substrate and would yield higher pumping rates for longer times during discharges. In order to test this hypothesis, the initial 2006-LITER evaporations ranging from 1.6 to 643 mg employed no wall preconditioning with helium ohmic discharges. Each of these lithium evaporations was followed by an L-mode LSND deuterium reference discharge, which exhibited no improvement in plasma performance. This is consistent with the above LPI results, and expected if it is assumed that the deposited lithium reacted with the residual fuel gas embedded in the graphite PFCs.

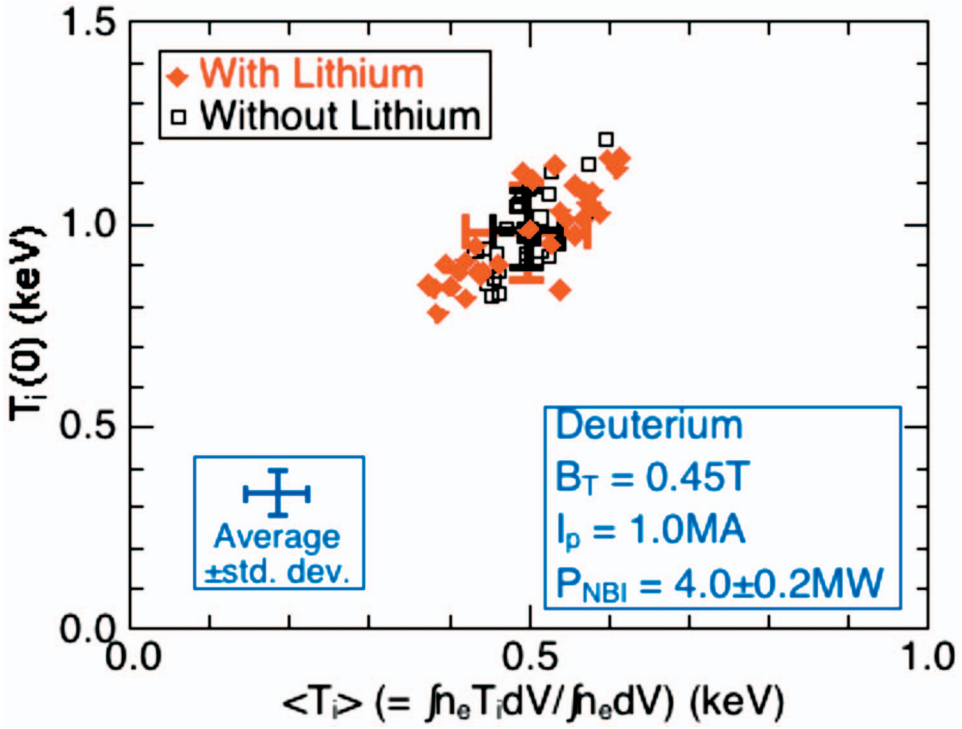

FIG. 8. (Color) Shown for the same discharges as in Fig. 6, is the central ion temperature $[T_i(0)]$ vs the volume-averaged ion temperature $[\langle T_i(0)\rangle]$ obtained by assuming the same density distribution (n_e) as the electrons.

2. 2006-LITER results for L-mode on conditioned graphite

Motivated by these results, subsequent evaporations were preceded by six ohmic helium wall conditioning discharges of the same shape as the following L-mode LSND NBI deuterium reference discharge (I_p=1 MA, P_{NBI}=4 MW, B_T=0.45 T). In these cases, there were immediate frequent small decreases in the line-averaged density (n_e) (e.g., ~15%), and increases in the associated electron temperature (T_e), ion temperature (T_i), electron stored energy (W_E), and energy confinement time (τ_E). The wall conditioning aspect of this result is consistent with the 2005-LPI results for similar L-mode plasmas, for which helium discharge conditioning was required prior to lithium deposition, for improvements in plasma performance. Nevertheless, in spite of relatively large total lithium deposition (≥600 mg) prior to the following deuterium reference discharge, the improvement in plasma conditions persisted for only one discharge.

3. 2006-LITER initial H-mode results using thicker lithium coatings on unconditioned graphite

The evaporations during the 2006-LITER campaign were used to test higher density H-mode reference discharges under lithium wall conditions using thicker lithium coatings on unconditioned graphite. In these experiments, it was found that, contrary to the L-mode behavior, improvements in the higher density H-mode deuterium reference plasma (I_p=1 MA, P_{NBI}=4 MW, B_T=0.45 T) were observed without first preceding the discharge with helium discharge conditioning. As before, however, these improvements in performance lasted for only about one discharge. This lack of need of helium discharge preconditioning, contrary to previous L-mode results, indicated that thicker lithium coatings obviated the need for thorough degassing of the graphite substrates, and possibly NSTX H-mode edge conditions may be more sensitive than L-mode edge conditions to the effects of active lithium. Consistent with this, in order to yield this improvement in discharge pumping, stored energy, and other characteristics, a minimum lithium deposition in the range of about 400 to 600 mg was required. In addition, minimizing the duration between the end of the evaporation and the succeeding deuterium reference discharge also yielded more frequent improvements in discharge pumping, stored energy, and other characteristics. Longer term changes in performance included a reduction in Z_{eff} $(r=0)$ due to reduced carbon in the core, which decreased as lithium recycling light deceased with discharge number, and a decrease in core oxygen light to levels at or below those directly following boronization. Dα luminosity was reduced by 70% during the 1st deuterium reference discharge following a lithium deposition sequence, and slowly increased in the following discharges without additional lithium deposition.

4. 2007-LITER H-mode results using higher lithium deposition rates and thicker lithium coatings on unconditioned graphite

The 2006-LITER experiments deposited up to a factor of 40 more lithium (~1 g), between reference deuterium discharges than in the 2005-LPI experiments (25 mg), and the cumulative total lithium deposition by the end of the 2006 campaign was about a factor of 90 more lithium. The 2007-LITER experiments typically deposited about the same amount of lithium (~1 g) between deuterium reference discharges (I_p=1 MA, P_{NBI}=4 MW, B_T=0.45 T), and the cumulative total was a factor of about 930 more than the 2005-LPI experiments, but provided in continuous deposition

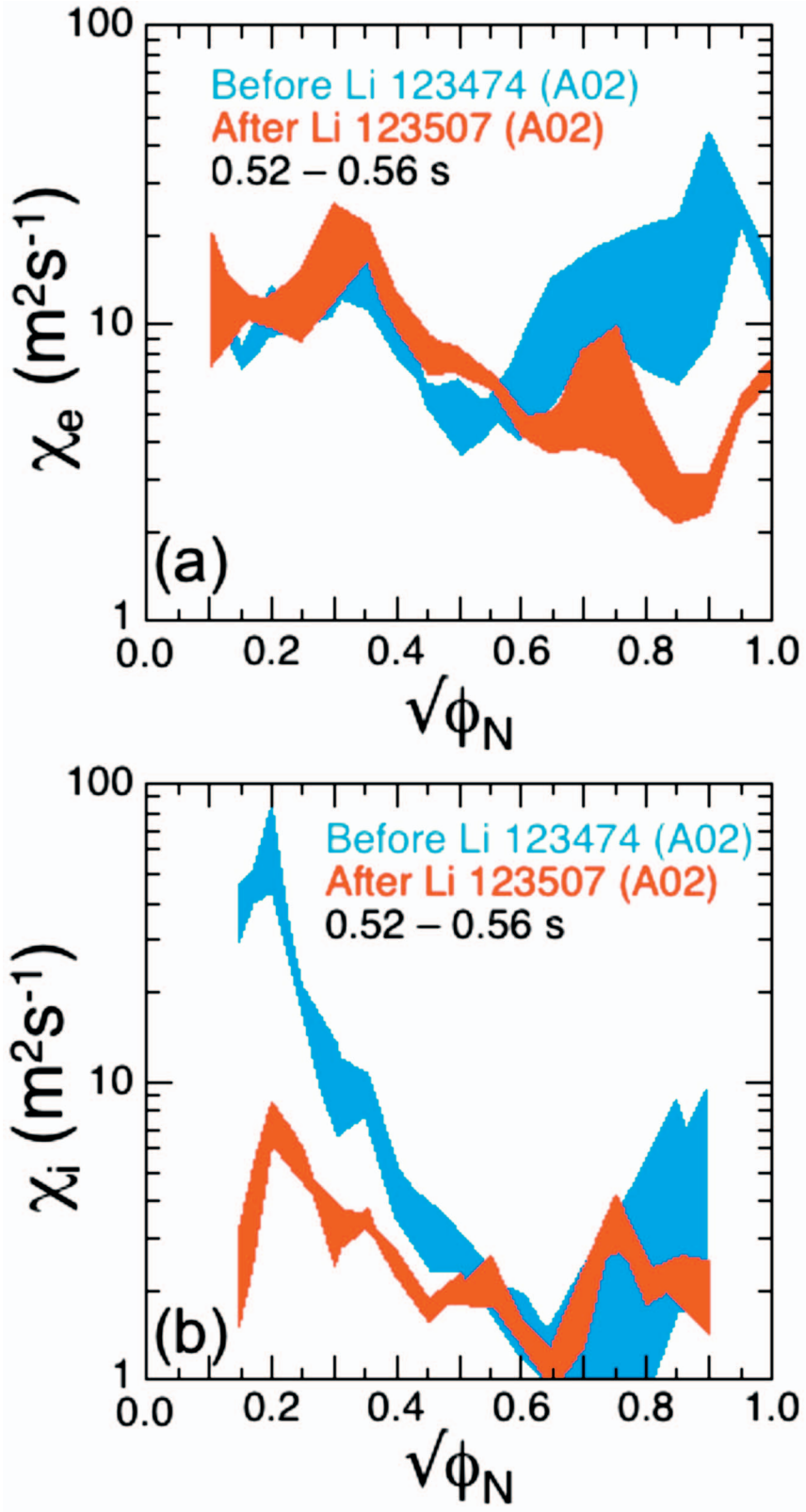

FIG. 9. (Color) Comparison of examples of (a) electron transport coefficients (χ_e) and (b) ion transport coefficients (χ_i) derived, respectively, using the time dependent transport code TRANSP for a quiescent interval in a discharge following lithium deposition with the same interval in a prior to lithium deposition discharge.

between and during discharges. Figure 6 shows the 2007-LITER database of electron stored energy (W_e) versus total stored magnetohydrodynamic (MHD) energy (W_{MHD}) for deuterium fiducial reference plasmas immediately following Li deposition, and for deuterium fiducial reference discharges prior to the start of lithium depositions. Shown also are the averages and standard deviations of the two groups of points. It is seen that, on average, the total stored energy is higher after lithium deposition, and that this is mostly through an increase in electron stored energy. Figure 7(a) shows for the same discharges, the central electron temperature $[T_e(0)]$ versus the volume-averaged electron temperature

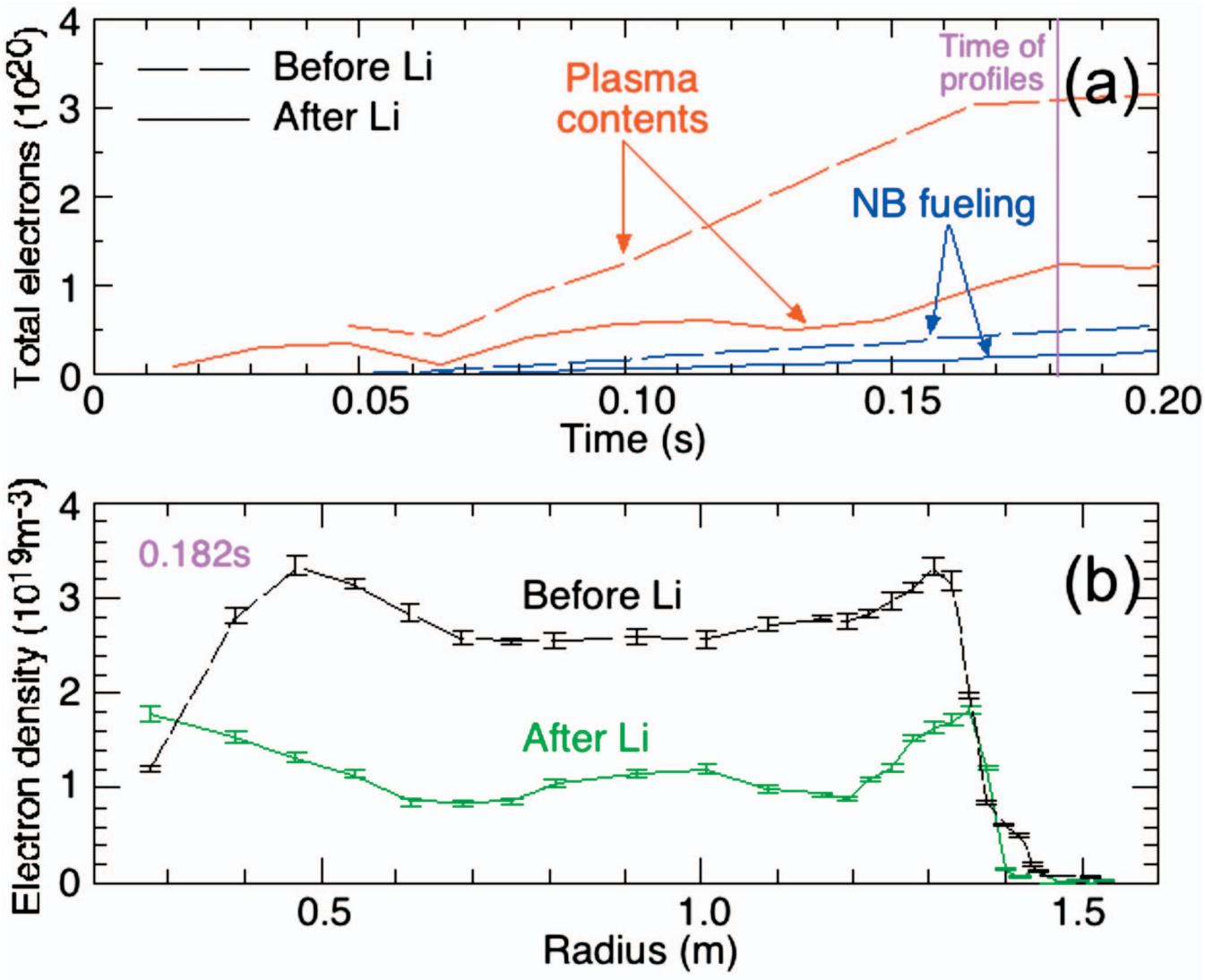

FIG. 10. (Color) Shown for deuterium reference discharges before and after Li deposition are (a) the total electron density and NB fueling waveforms and (b) the early density profiles at 0.182 s. Significant initial D pumping was exhibited at plasma start-up, at higher Li evaporation rates (35 mg/min). Prior to these discharges, typical Li evaporation rates of 10–20 mg/min were used.

$[\langle T_e \rangle]$. The central electron temperature $[T_e(0)]$ shows little change but that the volume-averaged electron temperature $[\langle T_e \rangle]$ increases after lithium deposition. Figure 7(b) shows the central density $[n_e(0)]$ versus the volume-averaged electron density $[\langle n_e \rangle]$. There is a slight broadening of the electron density profile $[\langle n_e \rangle]$ after lithium deposition. Figure 8 shows for the same discharges, the central ion temperature $[T_i(0)]$ versus the volume-averaged ion temperature $[\langle T_i(0) \rangle]$ obtained by assuming the same density distribution (n_e) as the electrons. There is no evident effect on the ion temperatures after lithium deposition. Figures 9(a) and 9(b) compare examples of electron transport coefficients (χ_e) and ion transport coefficients (χ_i) derived using the time-dependent transport code TRANSP.[9] They are for a quiescent interval in a discharge following Li deposition and the same interval in a discharge prior to lithium deposition. The edge χ_e and the core χ_i tend to decrease following lithium deposition consistent with a broadening of the $\langle n_e \rangle$ profile. Figure 10 shows significant deuterium pumping at the initial plasma start-up, at higher Li evaporation rates (35 mg/min). Prior to these discharges, typical lithium evaporation rates of 10 to 20 mg/min were used. A noteworthy observation during this work has been the influence of lithium wall conditions on edge-localized mode (ELM) and magnetohydrodynamic (MHD) behavior. Figure 11 shows an example of the reduction in ELM occurrence and periods of edge quiescence following lithium deposition. It is seen in this example that after lithium deposition, the stored energy W_{MHD} increased and the occurrence of large ELMs was greatly reduced. Note the quiescent period exhibited in the edge Dα luminosity in the interval 0.3 to 0.8 s. With increasing lithium deposition on the PFCs during the campaign day, the edge Dα, C II, and O II luminosity decreased (Fig. 12).

Typically, to facilitate reproducible plasma start-up conditions, HeGDC is applied between discharges for about 9 min to remove near-surface molecular deuterium from the graphite walls prior to the next discharge. This practice was followed during the 2007-LITER campaign to partially de-

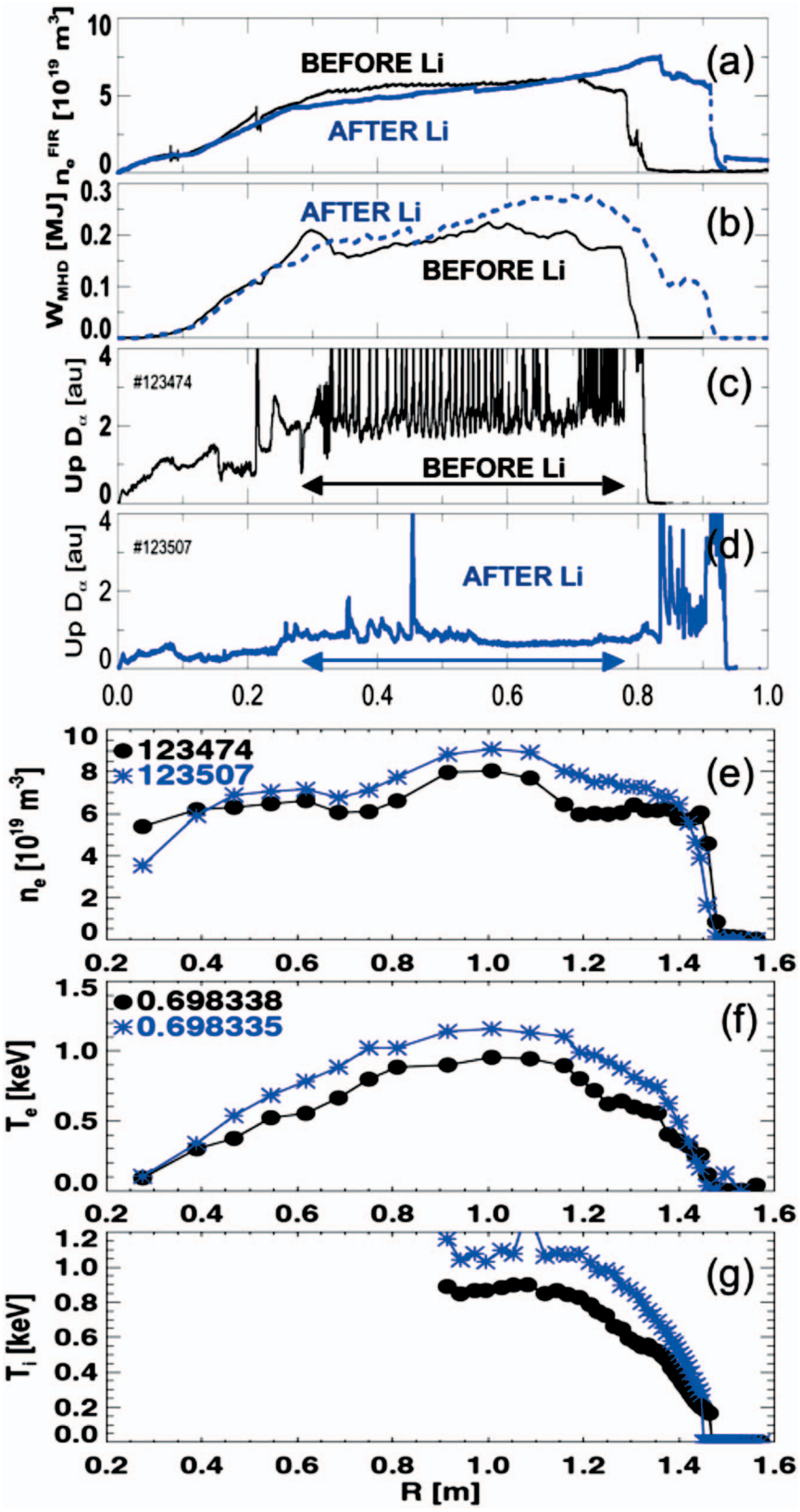

FIG. 11. (Color) Shown for two deuterium reference discharges before and after Li deposition are (a) the total electron density, (b) the stored energy, (c) Dα before Li, (d) Dα after Li, (e) density profile (0.698 s), (f) electron temperature profile (0.698 s), and (g) the ion temperature profile (0.698 s). After Li deposition the stored energy W_{MHD} increased (b) and the occurrence of large ELMs was greatly reduced (d). Note the quiescent period exhibited in the edge Dα luminosity (d) in the interval 0.3–0.8 s.

gas graphite PFCs as much as possible from the preceding discharge before the following discharge (~15 min duty cycle). Since LITER continued to evaporate during the HeGDC, this was effectively the process known as "lithiumization" (similar to boronization), whereby lithium atoms entering the HeGDC are ionized and deposited globally by the applied GDC bias (~400–600 V). While this lithiumization deposited lithium more globally, it also resulted in the co-deposition of helium and lithium, which slowly outgassed during the subsequent deuterium discharge. This effect has been measured previously, and is attributed to helium trapping in solid lithium interstitial voids.[10] The subsequent out-

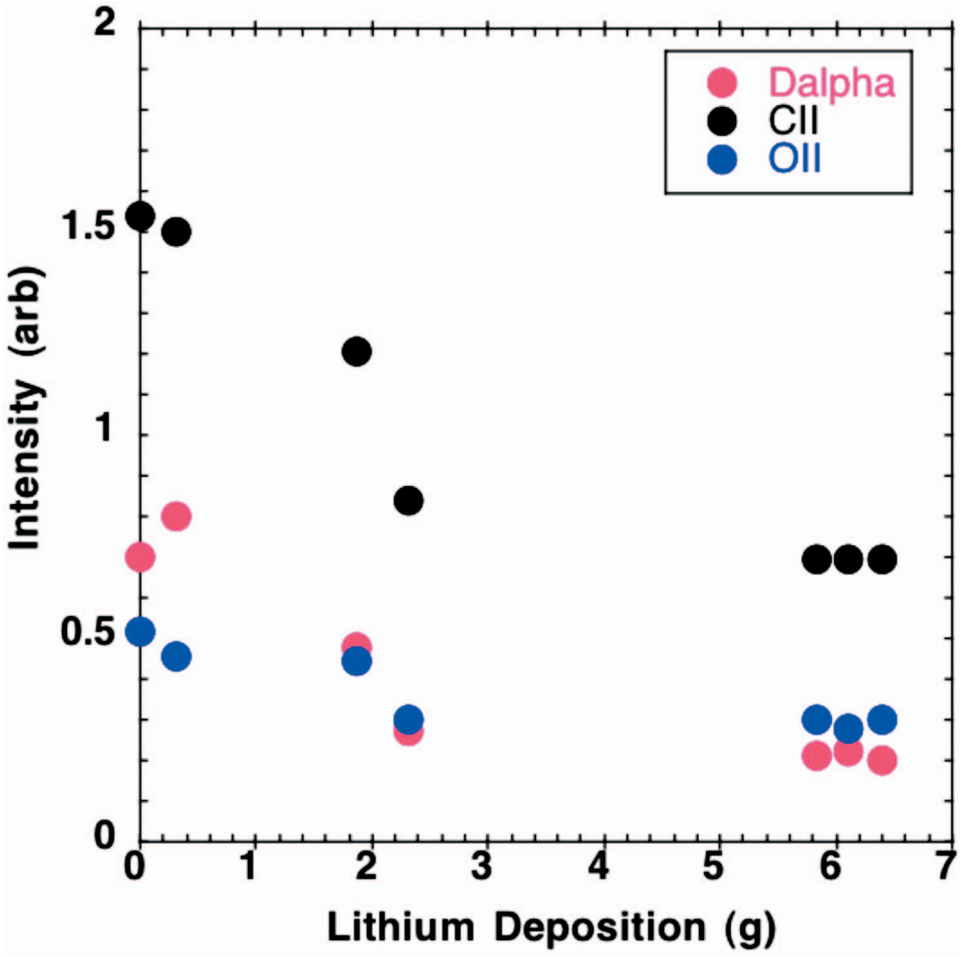

FIG. 12. (Color) The lower divertor Dα, C II, and O II luminosity decreased with increasing total accumulating lithium deposited on PFCs during the run day.

gassing is on the time scale of tens of minutes. Due to this trapped helium outgassing, the helium luminosity increased with discharge number as the total lithium deposition increased.

C. Results of sample analysis after venting the vessel

After venting the vessel to atmosphere, nuclear reaction analysis was performed to measure the concentration of deuterium versus depth using $D(^3He,p)\alpha$ reactions and the concentration of lithium versus depth using $^7Li(p,\alpha)\alpha$ reactions on a poloidal array of graphite tiles through the lithium deposition vertical plane. The deuterium coverage was found to be in the range $\sim 10^{17}$ to $>10^{19}$ D/cm^2, with the highest coverage ($>10^{19}$ D/cm^2) extending to depths beyond the range of analysis; i.e., >4 μm at the corner between the lower stack shoulder and the inner horizontal divertor. This was essentially the private flux region between the strike points for much of this work. Elsewhere, the deuterium concentration was within 4 μm of the surface. The lithium coverage is present on all tiles the range from $\sim 10^{17}$ to 10^{19} Li atoms/cm^2. The lithium coverage was $\sim$90% lower on tiles in the lithium shadow provided by the center stack than on unshadowed tiles within line-of-sight from LITER at similar poloidal locations, and the deuterium coverage was similar. This indicates that the D toroidal coverage was not greatly changed by lithium deposition (this result includes embedded deuterium from other nonlithium experiments performed during the campaign). The deposited lithium was measured to be within 5 μm of the surface everywhere on the line-of-sight surfaces; on tiles with low coverage, the lithium was within 2 μm of the surface. This shows the lithium did not diffuse into the graphite beyond a few micrometers. The nuclear reaction analysis indicates that this lithium appears to reside in a mixed concentration of presently unknown components; the possibility that these components could be carbon or oxygen is being investigated. X-ray photoelectron spectroscopy (XPS) was performed on surface region of some of the same divertor region tiles showed the presence of C, O, B, and Li. XPS spectral line shifts along various points on the same tiles, and between adjacent tiles, indicated chemical changes that are under investigation. Lithium oxide (Li_2O) formation was not evident in the XPS spectra. A strong presence of lithium hydroxide (LiOH) and lithium carbonate (Li_2CO_3) was exhibited. A systematic experimental uncertainty was introduced in such measurements by the present need to remove the samples after venting the vessel, and thereby allowing atmospheric reactions with the sample surfaces to change the vacuum conditions.

IV. DISCUSSION

The behavior of ions and neutrals incident on solid Li to form LiD provides a pumping effect studied in this work.[11] In the case of lithium pellet injection into diverted plasmas, the lithium is deposited toroidally along the plasma wetted region. In NSTX high triangularity diverted discharges with high flux expansion, this embodies the strike points and much of the inner and outer divertors. The lithium pellet deposition, whether via injection into the deuterium discharge of interest, or into preceding ohmic helium discharges, can provide only a thin lithium layer. This is due to the inability of plasmas to accept more than a few milligrams of injected lithium per discharge and remain unperturbed. Lithium evaporation from one evaporator prior to the discharge can provide lithium depositions on the divertor wetted region up $100\times$ or more. This is thicker than what LPI provides, but with less than complete toroidal coverage unless several evaporators are used. The amount of incident deuterium ions and neutrals that can be pumped by a solid lithium coating on the plasma wetted area is determined by the depth range of the incident particles. At typical NSTX plasma energies, the range of deuterium is about 100 to 250 nm.[12] As the central lithium thickness directly under LITER increases, the coating of regions far from LITER grow in sufficient thickness to stop incident particles and form LiD, and hence, the effective pumping area is extended. Nuclear reaction analysis of graphite tiles after venting found the deposited lithium did not diffuse into the graphite beyond a few micrometers. This is in contrast to previous laboratory measurements which found rapid diffusion of lithium into bulk graphite.[13] However, previous laboratory measurements of lithium diffusion in graphite may not be representative of present NSTX graphite conditions. The effects, for example, of repeated NSTX boronizations since 2000, and the formation of lithium compounds may inhibit diffusion into the graphite substrate. The lithium measurements in this work found that the rate of lithium deposition and the duration to the subsequent deuterium discharge were important for achieving stronger and more reproducible lithium effects. This suggests that faster deposition rates and shorter exposure times minimize the time allowed for lithium to react in a manner that reduces the amount of fresh atomic lithium available to form LiD with the incident deuterium efflux. Work is in progress to determine the relative contributions of the effects of lithium interactions with the exposed NSTX divertor graphite, and the contributions to the residual vacuum partial pressures (e.g., H_2O, CO, CO_2) during the experimental campaign, and subsequent exposure to atmosphere after the vessel venting.

The application of HeGDC during lithium evaporation to facilitate plasma start-up conditions results in a previously measured co-deposition uptake of helium, at a rate of 1.6×10^{14} He atom/cm^2/s to average atomic ratios of He/Li ~0.008 in the resultant co-deposits.[10] The slow outgassing of this co-deposited helium relative to the duty cycle allows for accumulation and the observed increase of helium in deuterium discharges with increasing discharge number. Future experiments will investigate the merits of possibly eliminating the need for this HeGDC by increasing the lithium deposition sufficiently to cover the D_2 from the preceding discharge.

The effect on plasma pumping, and performance of injected lithium pellets and lithium evaporated coatings applied immediately prior to the deuterium reference discharge exhibited beneficial improvements to discharge characteristics. The improvements included *decreases* in plasma density, inductive flux consumption, and ELM occurrence, and *increases* in electron temperature, ion temperature, energy confinement, and quiescent time. The work still in progress includes investigation of the origin of the continued secular density rise (i.e., small initial decrease in n_e, followed by a secular rise), the nature and duration of the lithium coatings, the reduction in ELM occurrence and discharges with periods of edge and MHD quiescence, helium retention following HeGDC (and perhaps eliminating HeGDC), diagnostic window depositions, and operational issues with improved confinement (e.g., increasing impurity confinement and core impurity radiation with discharge duration). In conclusion, while additional work is required to resolve the issues encountered, the NSTX high-power divertor plasma experiments have shown, for the first time, that benefits from lithium coatings applied to plasma facing components found previously in Tokamak Fusion Test Reactor (TFTR) limited plasmas can occur also in high-power diverted configurations.

ACKNOWLEDGMENTS

We acknowledge the technical contributions of S. Jurczynski, T. Provost, L.Guttadora, J. Taylor, S. Gifford, J. Desandro, J. Kukon, T. Czeizinger, J. Winston, L. Gernhardt, and P. Sichta. This work is supported by United States Department of Energy (U.S. DOE) Contract Nos. DE-AC02-76CH03073 (PPPL) and DE-AC05-00OR22725 (ORNL), those of Lawrence Livermore National Laboratory in part under Contract No. W-7405-Eng-48 and in part under Contract No. DE-AC52-07NA27344, and that of Sandia, a multiprogram laboratory operated by Lockheed Martin Company for the United States Department of Energy's National Nuclear Security Administration under Contract No. DE-AC04-94AL85000.

[1] M. Ono, S. M. Kaye, Y.-K. M. Peng, G. Barnes, W. Blanchard, M. D. Carter, J. Chrzanowski, L. Dudek, R. Ewig, D. Gates, R. E. Hatcher, T. Jarboe, S. C. Jardin, D. Johnson, R. Kaita, M. Kalish, C. E. Kessel, H. W. Kugel, R. Maingi, R. Majeski, J. Manickam, B. McCormack, J. Menard, D. Mueller, B. A. Nelson, B. E. Nelson, C. Neumeyer, G. Oliaro, F. Paoletti, R. Parsells, E. Perry, N. Pomphrey, S. Ramakrishnan, R. Raman, G. Rewoldt, J. Robinson, A. L. Roquemore, P. Ryan, S. Sabbagh, D. Swain, E. J. Synakowski, M. Viola, M. Williams, J. R. Wilson, and NSTX Team, Nucl. Fusion **40**, 557 (2000).

[2] M. G. Bell, R. E. Bell, D. A. Gates, S. M. Kaye, H. Kugel, B. P. LeBlanc, F. M. Levinton, R. Maingi, J. E. Menard, R. Raman, S. A. Sabbagh, D. Stutman, and the NSTX Research Team, Nucl. Fusion **46**, S565 (2006), and references therein.

[3] Fusion Eng. Des. **72**, 1 (2004). A large section of the "Special Issue on Innovative High-Power Density Concepts for Fusion Plasma Chambers" highlighted progress in this effort, and it continues as a primary focus of the United States Department of Energy (USDOE) "Advanced Limiter/Divertor Plasma-Facing Components (ALPS)" program.

[4] D. K. Mansfield, D. W. Johnson, B. Grek, H. W. Kugel, M. G. Bell, R. E.

Bell, R. V. Budny, C. E. Bush, E. D. Fredrickson, K. W. Hill, D. L. Jassby, R. J. Maqueda, H. K. Park, A. T. Ramsey, E. J. Synakowski, G. Taylor, and G. A. Wurden, Nucl. Fusion **41**, 1823 (2001).
[5]R. Majeski, S. Jardin, R. Kaita, T. Gray, P. Marfuta, J. Spaleta, J. Timberlake, L. Zakharov, G. Antar, R. Doerner, S. Luckhardt, R. Seraydarian, V. Soukhanovskii, R. Maingi, M. Finkenthal, D. Stutman, D. Rodgers, and S. Angelini, Nucl. Fusion **45**, 519 (2005).
[6]H. W. Kugel, R. Maingi, M. Bell, D. Gates, K. Hill, B. LeBlanc, D. Mueller, R. Kaita, S. Paul, S. Sabbagh, C. H. Skinner, V. Soukhanovskii, B. Stratton, and R. Raman, J. Nucl. Mater. **337–339**, 495 (2005).
[7]G. Gettelfinger, J. Dong, R. Gernhardt, H. Kugel, P. Sichta, and J. Timberlake, *Proc. 20th IEEE/NPSS Symposium on Fusion Engineering*, 359, San Diego, CA, 14–17 October 2003 (IEEE, Piscataway, NJ, 2003), IEEE Catalog No. 03CH37469, ISBN 0-7803-7908-X/03).
[8]H. W. Kugel, M. G. Bell, R. Bell, C. Bush, D. Gates, T. Gray, R. Kaita, B. Leblanc, R. Maingi, R. Majeski, D. Mansfield, D. Mueller, S. Paul, R. Raman, A. L. Roquemore, S. Sabbagh, C. H. Skinner, V. Soukhanovskii, T. Stevenson, and L. Zakharov, J. Nucl. Mater. **363–365**, 791 (2007).
[9]R. J. Hawryluk, in *Physics of Plasmas Close to Thermonuclear Conditions*, edited by B. Coppi G. G. Leotta, D. Pfirsch, R. Pozzoli, and E. Sindoni, Pergamon, Oxford, 1980), Vol. 1, p. 19.
[10]Y. Hirooka, S. Hosaka, M. Nishiura, Y. Ohtsuka, and M. Nishikawa, J. Nucl. Mater. **363–365**, 775 (2007).
[11]M. J. Baldwin, R. P. Doerner, S. C. Luckhardt, and R. W. Conn, Nucl. Fusion **42**, 1318 (2002).
[12]J. N. Brooks, J. P. Allain, T. D. Rognlien, and R. Maingi, J. Nucl. Mater. **337–339**, 1053 (2005).
[13]N. Itou, H. Toyoda, K. Morita, and H. Sugai, J. Nucl. Mater. **290–293**, 281 (2001).